Measurement of the 100 nm NIST SRM® 1963 by laser surface light scattering

Thomas A. Germer,[a] George W. Mulholland,[a] Jung Hyeun Kim,[a,b] and Sheryl H. Ehrman[b]

[a]*National Institute of Standards and Technology, Gaithersburg, MD 20899*
[b]*Department of Chemical Engineering, University of Maryland, College Park, MD 20742*

ABSTRACT

Accurate sizing of particles deposited on surfaces is important for the semiconductor, optical, and data storage industries. The recent availability of accurate light scattering models for non-ideal conditions enables the determination of particle size with a complete assessment of the measurement uncertainties. In this manuscript, we describe a light scattering measurement of the National Institute of Standards and Technology (NIST) Standard Reference Material (SRM®) 1963 deposited onto a silicon wafer. The measurement was carried out using 441.6 nm, p-polarized light. The measurement yielded a value of 99.7 nm with an expanded uncertainty (95 % confidence limit) of 1.7 nm. The uncertainty is dominated by the reproducibility of the measurement. Uncertainties in the substrate optical properties, the thickness and optical properties of the substrate oxide, and the shape of the particle dominate the systematic uncertainty.

Keywords: calibration, inspection, particles, PSL, scattering, size, spheres

1. INTRODUCTION

Light scattering is used by the semiconductor, optical, and data storage industries to inspect materials for surface quality.[1] Light scattering instruments often require calibration with well-characterized scattering artifacts such as surfaces with roughness[2] or deposited particles.[3] Because all measurements performed after calibration rely upon that calibration being accurate, the accuracy of those measurements is only as good as that used for the calibration. While this accuracy may seem to be simply a constant proportionality, many instruments rely upon ratios of signals obtained on different detectors to determine the nature of the scatterer.[3] It has been found that small uncertainties in the scattering artifact standard can lead to unacceptable errors in the interpretation of the scattered light.[4] Furthermore, since the size distribution of naturally occurring particles increases with decreasing size, a small change in a tool's calibration can lead to relatively large change in the number of particles above an acceptable size counted. Since tolerable contamination levels are often specified for starting wafers, accurate size standards are required so that wafer vendors and integrated circuit manufacturers can agree on the quality of materials being delivered.

Recent improvements in the measurement and calculation of scattering by small particles bound to surfaces has enabled the certification of artifacts containing predeposited particulate contaminants.[3,5] Certification for particle size implies that an uncertainty budget can be placed on the measurement. Thus, the scattering must be understood well enough that all the different sources of uncertainty can be analyzed. The theoretical models available now provide essentially exact solutions to the Maxwell equations for a sphere on a surface, and can provide quality results for many non-ideal particles.[6–8] Thus, it is possible to use these models to assess the uncertainty in the measurements.

In this Proceeding, we discuss a measurement of the National Institute of Standards and Technology (NIST) Standard Reference Material, SRM® 1963, which consists of polystyrene latex spheres with a nominal diameter of 100 nm, suspended in an aqueous solution.[9] There is interest in measurements of the diameters of these particles after they have been deposited on wafers. A light scattering measurement of SRM® 1963 on silicon wafers was performed by a commercial firm, The Scatter Works (TSW),[10] using a method similar to that used here.[5] The success of their work partially motivated the work described here. We have identified a number of sources of measurement uncertainty that were not considered by the previous study and that can dominate the combined uncertainty under some conditions.

2. THEORY

We use the theory of Bobbert and Vlieger[6] (BV) to evaluate the scattering of light by a sphere on a substrate. The theory extends the Mie scattering solution for a free-space particle by self-consistently including the reflection of the scattered waves in the incident excitation. While the original theory did not consider the existence of layers on either the substrate or the particle, addition of these effects are self-apparent from their discussions.[11] That is, the solution is given with respect to the reflection coefficients of the substrate and the Mie scattering coefficients. The respective coefficients for a coated substrate or for a coated sphere are known and can be used in the calculation. A complete description of the implementation of the theory is described elsewhere.[12] The success of this theory has been well established,[11] and our implementation of it has been made available as part of the SCATMECH library of scattering codes.[13] The implementation for the spherical particle is sufficiently fast that it is possible to perform non-linear least squares fits to data, letting the particle density and diameter be free parameters. Furthermore, the theory can be extended to axially symmetric particles and arbitrarily shaped particles relatively straightforwardly using the T-matrix approach.[8,14] Table I presents the nominal parameters used in the calculation and the fits.

Table I. Parameters used in the simulations and the fits. The uncertainties in these values are discussed in Sec. 4.

Parameter	Symbol	Value
Wavelength	λ	441.563 nm
Incident angle	θ_i	60°
Scattering angles	θ_r	–50° to 50° in steps of 5.3°
Sphere index	n_{PSL}	1.617
Substrate index	n_{Si}	4.7976+0.0901i
Native oxide thickness	τ	1.9 nm
Native oxide index	n_{ox}	1.590

3. EXPERIMENT

NIST SRM® 1963 consists of a suspension of carboxylated polystyrene spheres in deionized filtered water. The mass concentration of spheres is approximately 5 %. The spheres were diluted by adding one drop of the suspension to 2000 mL of deionized and filtered water (0.2 μm pore size) before being nebulized. After drying, the aerosolized spheres were passed through a differential mobility analyzer (DMA) classifier, whose voltage and flow conditions were set to maximize the throughput of particles. Since the distribution of particles (standard deviation of 2.2 nm) was narrower than the DMA pass-band (20 nm), the DMA had little effect on the distribution of sphere sizes, but served to reduce the number of doublet and residue particles. The fraction of aerosol droplets containing multiple spheres was determined to be approximately 0.01. The aerosol stream was then sent to an electrostatic precipitator, which deposited the particles onto a 2.54 cm diameter silicon wafer. The silicon wafer was cleaned using a standard cleaning procedure before the deposition process.

Measurements of the scattering of light by the dilute surface concentration of spheres deposited upon silicon wafers were carried out using the Goniometric Optical Scatter Instrument described elsewhere.[15] The wavelength used was that from a helium-cadmium laser at 441.563 nm. While the instrument has full polarimetric capabilities, we removed all polarization optics from the system, with the exception of a polarizer on the incident laser beam, in order to reduce uncertainties resulting from the polarization measurement. Furthermore, all measurements were carried out using a fixed incident angle $\theta_i = 60°$, scanning the scattering angle from $\theta_r = –50°$ to $\theta_r = 50°$ in 5.3° steps, remaining in the plane of incidence. Measurements of the bidirectional reflectance distribution function (BRDF) were carried out on two samples, the wafer containing spheres and on another clean witness wafer, each at nine different locations. The BRDF measured by the witness wafer includes the effect of scattering by surface roughness and the instrument signature, the latter of which dominates the signal and results from Rayleigh scattering in the air surrounding the sample.[16] The measurements from the witness wafer were averaged before being subtracted from the signals obtained on the wafers with spheres. Two of the measurements on the wafers with spheres had significant deviations from the other measurements, presumably from foreign particles, and were discarded. Figure 1 shows the measured BRDF obtained from

the remaining seven locations on the wafer surface after correcting for the signal from the witness wafer. The signals from the witness wafer before averaging are also shown to illustrate the magnitude of the correction.

The data sets for each location were individually fit to the scattering model using a Levenberg-Marquardt nonlinear least squares algorithm.[17] Table II shows the resulting values obtained from each set and the resulting weighted mean and uncertainty. The specified uncertainties, u_D and u_ρ, include only the uncertainty obtained from the curvature of χ^2 determined during the nonlinear least squares fit.

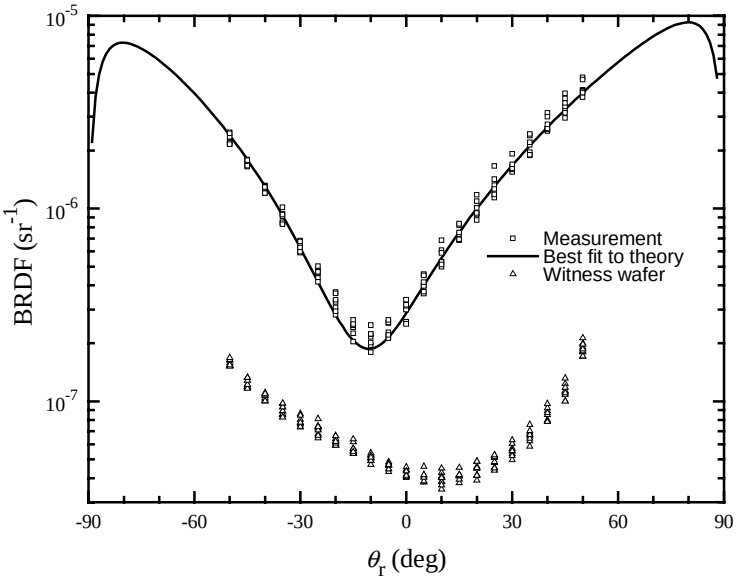

Figure 1. Light scattering of p-polarized light by PSL spheres on a silicon substrate measured in the plane of incidence at five different locations (squares). The solid curve represents the best fit to the theory as described in the text.

Table II. Results of fits to the data. The uncertainty represents the standard uncertainty.

Location	D (nm)	u_D (nm)	ρ (mm^{-2})	u_ρ (mm^{-2})
1	98.77	0.84	7 100	370
2	100.14	0.99	6 910	420
3	99.40	0.73	6 660	300
4	100.81	0.90	6 400	350
5	103.10	1.00	6 490	400
6	103.30	1.20	5 810	400
7	102.40	1.20	6 500	480
Weighted Mean:	100.67	0.67	6 570	150

4. PARTICLE SIZE UNCERTAINTY ESTIMATE

In this section, we attempt to determine the uncertainty and any corrections in the measured diameter of the particles deposited on the surface. To perform this estimate, simulations of the data were performed for specific non-ideal conditions, considered to be perturbations on the ideal case. The simulated results were then fit to the ideal model using the nominal parameters. These fits result in the estimated sensitivity for each parameter. The nominal values used for the fits, and for which perturbations were centered, are given in Table I. In the following, we discuss each source of uncertainty that we could identify. The model used to fit the data did not include the effects for some of the parameters, such as size polydispersity and particle non-sphericity. Addition of these parameters contributes correction factors to the model fits.

Uncertainties can be divided into those obtained by a statistical analysis (Type A) and those obtained using other means (Type B), which are usually considered systematic.[18] Estimates are made of the standard deviation, u_i, of the distribution for each possible error associated with each source. For those Type B uncertainties for which we obtain a tolerance, a range of values, or a maximum error, we assume a uniform distribution over the extents of that range. The standard deviation of a uniform distribution of half-width x is given by $x/\sqrt{3}$. All of the sources of uncertainty, u_i, are then added in quadrature, resulting in a combined standard uncertainty, u_c. Since the standard uncertainty represents a confidence level of 68 %, this quantity is multiplied by a coverage factor $k = 2$ to yield an expanded uncertainty, U, representing a confidence level of 95 %. In the following, we outline the contributions to the expanded uncertainty.

4.1. Random sources

The random sources of uncertainty result from detector noise, laser speckle, and the background instrument signature. The uncertainty from detector noise for the system used in this study was determined by multiple sampling and was found to be less than 0.5 % of the signal in the signal range of interest. Speckle noise, however, is much larger and depends upon the illuminated spot size, the collection solid angle, the wavelength, and, to a smaller extent, the degree of polarization of the scattered light. By measuring the effective uniformity of a non-depolarizing uniformly scattering sample (roughened black glass), the uncertainty from speckle noise was found to be approximately 4.2 % of the signal when viewing at the surface normal. The combined detector noise and speckle uncertainties were used to determine the weighting factors for each data point during the nonlinear least squares fits. The normalized-χ^2 values for the fits ranged from 1.2 to 3.6. The uncertainties from all of the random sources are included in the estimates of the uncertainties of the nonlinear least squares fits. The weighted mean is obtained using[19]

$$\langle x \rangle = \sum (x_i / u_i^2) / \sum (1/u_i^2), \tag{1}$$

where x_i are the data values and u_i are the associated estimates of their uncertainties. The standard deviation of the diameters shown in Table I, 1.69 nm, is significantly larger than the estimates of that standard deviation obtained from the nonlinear least squares fits. We determine the weighted uncertainty in the weighted mean using[19]

$$u^2 = \frac{N}{N(N-1)}\left[\sum (x_i^2 / u_i^2) / \sum (1/u_i^2) - \langle x \rangle^2\right], \tag{2}$$

where N is the number of data points. The standard uncertainty $u_D = 0.67$ nm is considered to include all of the Type A uncertainty in this measurement.

4.2. Indices of refraction of particles and substrate

Multiple values exist in the literature for the index of refraction of polystyrene at 441.6 nm. Marx and Mulholland[20] performed light scattering measurement of polystyrene spheres and obtained a variety of results between 1.599 and 1.619. The weighted mean and uncertainty of their results yields an index of 1.617 with a standard uncertainty of 0.002. The variation of the index by 0.002, leads to variation in the best fit of D by 0.04 nm. Thus, we assign a standard uncertainty of 0.04 nm to the effects of the particle index.

Herzinger *et al.*[21] have measured the optical constants for silicon using variable angle spectroscopic ellipsometry and provide a review of the various literature values that exist for these values. The values at 441.6 nm range from that reported by Palik[22] (4.768+0.166i) to Herzinger *et al.*[21] (4.798+0.090i). We chose to fit the data to the mean value of 4.783+0.128i, and examine the effects of uncertainty of n_{Si} of 0.015 and k_{Si} of 0.038. Variation in n_{Si} by 0.015 yields a variation in the measured D by 0.05 nm, while variation in k_{Si} of 0.038 yields a variation in the measured D by 0.39 nm. We treat these two uncertainties as independent, and having a uniform distribution between the extremes. Therefore, the standard uncertainties due to the substrate optical constants, n_{Si} and k_{Si}, are 0.03 nm and 0.23 nm, respectively.

4.3. Thickness and index of substrate oxide film

The native oxide of silicon has been reported to have a thickness τ which depends upon surface treatment and age, and reports of the optical constants of this layer, n_{ox}, vary. The measurement of the film thickness by ellipsometry depends upon the optical constant assumed for that layer. Ellipsometry effectively measures $n_{ox}^2\tau$. We performed spectroscopic ellipsometry on both the deposition wafer and the witness wafer to obtain a film thickness, and the results were identical for the two wafers. Using n_{ox} = 1.47, typical for a thermally-grown oxide, we obtained a thickness of 2.2 nm, while using n_{ox} = 1.74, which has been reported for the native oxide by Herzinger *et al.*,[21] we obtained a thickness of 1.6 nm. We fit the data using a root-mean-square value of the index (n_{ox} = 1.61) and a mean value of the thickness (τ = 1.9 nm). The shift in the particle diameter obtained by using one of the extreme thicknesses with its respective index is about 0.60 nm. Assuming a uniform distribution, we assign a standard uncertainty of 0.34 nm to effects of the oxide film.

4.4. Wavelength

It is perhaps not necessary to consider the uncertainty in the wavelength, but for completeness we calculate it based upon the gain bandwidth of the lasing media. The 441.563 nm HeCd laser line has a natural linewidth of about 2 GHz. Assuming the gain bandwidth is dominated by the natural linewidth of the Cd II atomic transition, the uncertainty in the wavelength is about 0.001 nm. The sensitivity of the particle size determination to the wavelength is found to be approximately 0.3 nm/nm. The wavelength of the laser therefore contributes insignificantly to the measurement uncertainty. (The index of refraction of air is approximately 1.00028 at 15 ºC and atmospheric pressure and is included in the wavelength.)

4.5. Particle shape

It is difficult to estimate the extent to which the free particles are spherical. Furthermore, it is difficult to predict how such a non-spherical shape is going to affect the scattering distribution. However, recent calculations indicate that it is the shape in the region near where the particle contacts the surface that is most important.[23] In this case, one must consider the deformation that is likely to occur when a deformable sphere adheres to a surface. Using the theory of Johnson, Kendall, and Roberts (JKR),[24] one can estimate the contact radius of a polystyrene sphere on a surface:

$$a_0 = (6\pi R^2 W / K)^{1/3}, \tag{3}$$

where W is the work of adhesion for the polystyrene/silicon dioxide surface, and

$$K = \frac{4}{3}\left(\frac{1-\nu_{sph}^{\ 2}}{E_{PS}} + \frac{1-\nu_{sub}^{\ 2}}{E_{sub}} \right)^{-1}, \tag{4}$$

where ν and E are Poisson's ratio and Young's modulus, respectively, for the sphere and substrate. Given values available in the literature, we find that

$$a_0 \cong 0.6\,(R/\text{nm})^{2/3}\ \text{nm} \tag{5}$$

This value can be used to estimate a dent distance,

$$\delta \cong 0.19(R/\text{nm})^{1/3}\ \text{nm}. \tag{6}$$

Thus, for a 100 nm sphere, the value of δ is approximately 0.7 nm. Inclusion of this effect shifts the apparent particle diameter by approximately 0.95 nm. This means that when a 100 nm sphere is slightly flattened by 0.7 nm, the best fit scattering analysis based on a spherical shape for the predicted flattened sphere scattering leads to a sphere size of 99.05 nm. The distortion given by Eq. (6) is expected to be an upper limit, that which one would expect if a sphere were pushed onto a surface with some force and then released. If little force or impact is applied to the particle upon deposition, this distortion may be significantly less. Therefore, we assume that the range of values for the possible cor-

rection extends from zero to 0.95 nm, that the correction to the particle diameter is the mean value, +0.48 nm, and that the standard uncertainty in this value is 0.27 nm.

4.6. Presence of doublet particles

A small fraction of the deposited particles were doublets (two attached spheres). Since the differential mobility analyzer passes particles based upon their volume to charge ratio, doublet particles which are doubly charged will pass through the analyzer with the singlet spheres which are singly charged. By measuring the ratio of singly-charged doublet particles to singly-charged singlets, and assuming that the charges on the particles are distributed according to Boltzmann statistics, the fraction of particles deposited on the wafer which are doublets was determined to be approximately 1 %, with a standard uncertainty of approximately 0.1 %. Since the intensity of scattering by small particles varies approximately as the square of the particle volume, these particles are expected to contribute approximately 4 % to the signal. It is difficult to assess the scattering from these particles, since their orientations on the surface are unknown. However, we would expect that their orientation distributions would lie between two extremes: oriented randomly with both particles touching the surface, and oriented with at least one sphere touching the surface and the other randomly distributed over a hemisphere. Discrete dipole calculations[25] were performed over ensembles of orientations to assess the scattering signals from each of these distributions. The net signal for each ensemble was then estimated for a number fraction of 1 % and added to calculations for a sphere. Resulting fits to a spherical particle yielded diameters larger by 1.06 nm and 1.19 nm, respectively. These corrections were found to be linear in the fraction of doublet particles. We therefore assume an average correction of −1.12 nm. Assuming a uniform distribution between the extremes, and including the uncertainty in the fraction, we find that the uncertainty arising from the presence of doublet particles is 0.17 nm.

4.7. Size polydispersity

The model used to fit the data assumes that all of the spheres are identical. The standard deviation of the width of the diameter distribution in SRM® 1963 has been measured to be approximately 2.2 nm by electron microscopy.[9] Since the intensity scattered by small particles is highly nonlinear in diameter D, any size polydispersity will have a tendency to make the particle diameter appear larger than its mean. If we assume that the particles have a size distribution given by $P(D)$, then we can estimate the scattering by assuming that the net BRDF $f_r'(\theta_i, \theta_r)$ is integrated over this distribution:

$$f_r'(\theta_i, \theta_r) = \int P(D)\, f_r(\theta_i, \theta_r | D)\, dD \tag{7}$$

where $f_r(\theta_i, \theta_r | D)$ is the BRDF for spheres of diameter D. Simulations using Eq. (7) were carried out using three different distribution functions with standard deviations of 2.2 nm: normal (Gaussian), log-normal, and triangular. The simulations yielded effective shifts of 0.30 nm, 0.32 nm, and 0.30 nm, respectively, and these shifts behave quadratically with the standard deviation of the distribution. While we do not have an uncertainty in the standard deviation of the distribution, we will assume that it is less than 0.5 nm. Due to the quadratic behavior of the shift with distribution width, this corresponds to a 40 % uncertainty in the correction factor. We therefore assume a correction to the particle diameter of −0.30 nm, with a standard uncertainty of 0.12 nm.

4.8. Geometrical errors

The absolute accuracy of the rotation stages is specified to be better than 0.02°. The sample is aligned in the sample mount by retroreflecting the laser beam at normal incidence. An iris centered on the incident beam and approximately 1 m from the sample is closed down, and the retroreflected beam is centered on it with a resolution of about 1 mm. The incident angle is thus aligned to the incident beam within 0.0005 mrad or 0.03°. The uncertainty in the incident angle is a combined uncertainty in the rotation stage accuracy and the alignment accuracy. Assuming that the distribution is

uniform over this range, the standard combined uncertainty in the incident angle is 0.02°. A simulation of a 0.02° error leads to a 0.05 nm uncertainty in the diameter measurement resulting from the incident angle.

The uncertainty in the scattering angle is dominated by uncertainties in the alignment of the goniometer axes and the matching of the sample surface to those axes. While the detector aperture used for the measurements subtended a half angle of approximately 0.35°, alignment was carried out using a co-aligned aperture with a half angle of 0.05°. The detector assembly is aligned to the incident beam with the sample removed to an accuracy of 0.02°. With the sample in place and varying the incident angle, the detector was able to follow the specular beam within 0.02°, providing an uncertainty resulting from the goniometer alignment. We combine the uncertainty from the rotation stage accuracy (0.02°), alignment of the incident angle (0.03°), alignment to the incident beam (0.02°), and the alignment of the goniometer axes (0.02°), providing a range of 0.046°, with uniform distribution. A simulation of a 0.027° error (that assuming a uniform distribution), uniformly applied to all scattering angles, leads to a 0.08 nm uncertainty in the diameter measurement from the scattering angle.

Since these particles scatter p-polarized light with significantly higher intensities than s-polarization, errors due to the incident polarization are expected to be fairly small. A 5° error on the incident polarization state direction (but still linearly polarized), for example, will lead to a 0.27 nm error in particle size, and the correction varies quadratically with the incident polarization angle. An estimate of the incident polarization state leads us to believe that the polarization is within 1° of p-polarization. Therefore, we assign the uncertainty in the particle diameter resulting from the uncertainty in the incident polarization state to be about 0.01 nm.

4.9. Focussing of the incident beam and the finite solid angle of collection

The optics in the scattering instrument are aligned so that the laser is focussed at the detector, providing the instrument with a high angular resolution. As a result, there is a distribution of incident angles on the sample, centered about the nominal incident angle. The convergence half-angle is approximately 0.5° and the beam waist at the sample is approximately 1 mm in diameter. We simulate the effect of the focussed incident beam by performing an integral over the directions contained in the incident beam, assuming that the angles of incidence and scattering are correlated to the position a ray strikes the sample, in a manner that is consistent with focussing of the incident beam onto the detector aperture. The integration is performed in an incoherent manner (integration of the intensity or Mueller matrix) to determine the scattering function. Using a top-hat beam profile, which represents a worst-case condition, we find that the fit using the nominal incident angle overestimates the particle diameter by 0.003 nm, and that this correction is quadratic in the convergence half-angle. We therefore find that the focussing of the incident beam does not contribute significantly to the measurement of the particle diameter.

The scattered light receiver views the sample with a solid-angle-defining aperture subtending a half-angle of 0.35°. Errors can occur if the BRDF varies strongly across the subtended detector angle. We performed a simulation to assess the correction that is necessary to account for a finite solid angle of detection, by performing integration over the right-circular solid angle of collection. The finite solid angle collected by the detector leads to an overestimation of D by 0.0013 nm, and the effect is quadratic in the half-angle of the detector. We therefore find that the finite solid angle of collection does not contribute significantly to the measurement of the particle diameter.

4.10. Detector linearity

In order to test linearity over a wide range of signal intensities, generally one must test a ratiometric signal over a wide range of signals. If the signal appears to be linear, then for each ratiometric measurement, an uncertainty can be stated for that linearity. When these results are pieced together to obtain the linearity over a wider dynamic range, these uncertainties add in quadrature. If we let L be a measured uncertainty of the linearity per decade, a reasonable expression for the uncertainty due to linearity over a larger range is

$$\Delta S_0 / S_0 = L\sqrt{\left|\log_{10}(S_1 / S_0)\right|}\,, \tag{8}$$

where S_0 and S_1 are the extreme signals, and ΔS_0 is the uncertainty in the signal S_0. For example, if the ratio of the signals is 100, then the relative uncertainty would be $\sqrt{2}\,L$, which is the quadrature sum of uncertainty gained in two decades. The value of L for the instrument used for this measurement was estimated to be 0.13 % per decade. This linearity is assumed to include all sources of linearity, including detector linearity, amplifier linearity, and scale change accuracy. Eq. (8), however, is not appropriate when the signals are such that the detector is near saturation; the uncertainties in a saturated region would not add incoherently. The effect of detector linearity on the measurement can be simulated by applying a nonlinear transformation to the signal,

$$S \leftarrow S \exp\left(L \log_{10} S\right), \tag{9}$$

which forces nonlinearity of L per decade. This simulation found a shift of 0.008 nm for L = 0.13 % per decade, and the effect was approximately linear in L.

4.11. Structure factor

One usually assumes that the BRDF is proportional to the density of the illuminated particles. However, for high particle densities and rough surfaces, interference between the scatter from the particles can lead to effects that couple the roughness function to the particle scattering function. That is, a structure factor must be considered. In the end, this effect is negligible, but we include the arguments for completeness. Assume that the field scattered by each scatterer if it were located at the origin is $\mathbf{E}_i$. Then the total field of a number of these scatterers, each located at some position $\mathbf{r}_i$ is given by

$$\mathbf{E}_{\text{tot}} = \sum_i \mathbf{E}_i \mathrm{e}^{\mathrm{i}\Delta\mathbf{k}\cdot\mathbf{r}_i} \ , \tag{10}$$

where $\Delta\mathbf{k} = \mathbf{k}_\mathrm{r} - \mathbf{k}_\mathrm{i}$ is the change in the wavevector of the light. If we assume that the scatterers are all identical, so that $\mathbf{E}_i = \mathbf{E}_0$, then

$$\mathbf{E}_{\text{tot}} = \mathbf{E}_0 \sum_i \mathrm{e}^{\mathrm{i}\Delta\mathbf{k}\cdot\mathbf{r}_i} \ . \tag{11}$$

The norm of the summation is often called the *structure factor*, while $|\mathbf{E}_0|^2$ is called the *form factor*. The structure factor is

$$S = \left|\sum_i \mathrm{e}^{\mathrm{i}\Delta\mathbf{k}\cdot\mathbf{r}_i}\right|^2 = \sum_i \mathrm{e}^{\mathrm{i}\Delta\mathbf{k}\cdot\mathbf{r}_i} \sum_j \mathrm{e}^{-\mathrm{i}\Delta\mathbf{k}\cdot\mathbf{r}_j} = \sum_i \sum_j \mathrm{e}^{\mathrm{i}\Delta\mathbf{k}\cdot(\mathbf{r}_i-\mathbf{r}_j)} = \sum_i 1 + \sum_i \sum_{j\neq i} \mathrm{e}^{\mathrm{i}\Delta\mathbf{k}\cdot(\mathbf{r}_i-\mathbf{r}_j)} = N + \sum_i \sum_{j\neq i} \mathrm{e}^{\mathrm{i}\Delta\mathbf{k}\cdot(\mathbf{r}_i-\mathbf{r}_j)} , \tag{12}$$

where N is the total number of particles. If we assume that the scatterers are uniformly distributed in x and y and bound to the surface, then the particle density function can be approximated by

$$\rho(\mathbf{R}) = \rho_0 \delta[R_\mathrm{z} - \zeta(\mathbf{R}_{xy})] \tag{13}$$

where ρ_0 is the surface density of scatterers, $\zeta(\mathbf{R}_{xy})$ is the surface height function, $\mathbf{R}_{xy}$ is the component of $\mathbf{R}$ in the mean surface plane, R_z is the component of $\mathbf{R}$ perpendicular to the mean surface plane, and $\delta(x)$ is the Dirac delta function. The second term in Eq. (12) can then be approximated by an integral

$$\begin{aligned} \sum_i \sum_{j\neq i} \mathrm{e}^{\mathrm{i}\Delta\mathbf{k}\cdot(\mathbf{r}_i-\mathbf{r}_j)} &\approx \left|\int d^3\mathbf{R}\rho(\mathbf{R}) e^{i\Delta\mathbf{k}\cdot\mathbf{R}}\right|^2 = \left|\rho_0 \int d^3\mathbf{R}\delta[R_\mathrm{z} - \zeta(\mathbf{R}_{xy})] e^{i\Delta\mathbf{k}\cdot\mathbf{R}}\right|^2 \\ &= \left|\rho_0 \int d^2\mathbf{R}_{xy} e^{i\Delta\mathbf{k}_{xy}\cdot\mathbf{R}_{xy}} \int dR_z \delta[R_\mathrm{z} - \zeta(\mathbf{R}_{xy})] e^{i\Delta k_z R_z}\right|^2 \\ &= \left|\rho_0 \int d^2\mathbf{R}_{xy} e^{i\Delta\mathbf{k}_{xy}\cdot\mathbf{R}_{xy}} e^{i\Delta k_z \zeta(\mathbf{R}_{xy})}\right|^2 \end{aligned} \tag{14}$$

If we assume that the surface height function is small compared to k_z, then we can make the approximation

$$\sum_i \sum_{j \neq i} e^{i\Delta\mathbf{k}\cdot(\mathbf{r}_i - \mathbf{r}_j)} \approx \left| \rho_0 \int d^2\mathbf{R}_{xy} e^{i\Delta\mathbf{k}_{xy}\cdot\mathbf{R}_{xy}} [1 + i\Delta k_z \zeta(\mathbf{R}_{xy})] \right|^2 . \quad (15)$$

Lastly, if we consider only diffuse scattering, so that $\Delta\mathbf{k}_{xy} \neq 0$, the first term in the integrand of Eq. (15) vanishes. We are then left with

$$\sum_i \sum_{j \neq i} e^{i\Delta\mathbf{k}\cdot(\mathbf{r}_i - \mathbf{r}_j)} \approx \left| \Delta k_z \rho_0 \int d^2\mathbf{R}_{xy} e^{i\Delta\mathbf{k}_{xy}\cdot\mathbf{R}_{xy}} \zeta(\mathbf{R}_{xy}) \right|^2 = A(\Delta k_z \rho_0)^2 S_2(\Delta\mathbf{k}_{xy}) , \quad (16)$$

where the power spectral density (PSD) function of the surface roughness is

$$S_2(\Delta\mathbf{k}_{xy}) = \lim_{A\to\infty} A^{-1} \left| \int_A d^2\mathbf{R}_{xy} e^{i\Delta\mathbf{k}_{xy}\cdot\mathbf{R}_{xy}} \zeta(\mathbf{R}_{xy}) \right|^2 . \quad (17)$$

Combining Eqs. (12) and (17), the structure factor per unit area is

$$S / A = \rho_0 [1 + \rho_0 (\Delta k_z)^2 S_2(\Delta\mathbf{k}_{xy})] . \quad (18)$$

If the surface is very flat or the density is sufficiently small, then the scattered signal should be proportional to the surface density. However, if the density is too high or the surface roughness too great, this value will be perturbed by the surface roughness. In fact, the particle scattering will mimic the surface roughness, since it has a term proportional to $S_2(\Delta\mathbf{k}_{xy})$. This issue is angle-dependent, so it will affect the shape of the scattering function. The polarization is not affected by the structure factor, which is to say that the polarization yields information about the form factor of the individual scatterer. Estimates of the surface roughness and particle surface density suggest that the effect of the structure factor is negligible for this measurement.

Table III: Summary of the uncertainties in the sphere diameter. All values are in nanometers. Unless otherwise specified, all uncertainties represent estimates of the standard deviation.

Type A (Statistical)		
Random uncertainties from fits		0.67
Type B (Systematic)		
Incident Angle		0.05
Scatter Angle		0.08
Linearity		0.01
Particle Index		0.04
Substrate (n)		0.03
Substrate (k)		0.23
Incident polarization		0.01
Substrate coating		0.34
Corrections:		
Particle shape	0.48	0.27
Doublet particles	-1.12	0.17
Polydispersity	-0.30	0.12
Total correction:	-0.94	
Combined standard uncertainty:		0.86
Total expanded uncertainty:		1.73

4.12. Summary of uncertainties

Table III shows a summary of all of the significant uncertainties in the measurement of the sphere diameter. The total expanded uncertainty ($k = 2$) is 1.73 nm. The total correction that must be applied to the particle size is –0.94 nm.

5. RESULTS AND DISCUSSION

The best fit to the spherical particle theory, with diameter $D = 100.67$ nm and surface density $\rho = 6\,570\ \mathrm{mm}^{-2}$, is shown as the solid curve in Fig. 1. The location of the minimum signal is the critical parameter affecting the determination of the particle size. After correction for particle shape and polydispersity we arrive at a diameter of 99.7 nm, with an expanded uncertainty of 1.7 nm. Figure 2 shows the results of several existing measurements of SRM® 1963. Measurements which include uncertainty analyses were performed by NIST using differential mobility analysis (NIST-DMA),[9] by NMIJ using an electro-gravitational aerosol balance (NMIJ-EAB),[26] by The Scatter Works[10] using surface light scattering (TSW-LS),[5] and by Duke Scientific[10] using transmission electron microscopy (DS-TEM). The NIST-DMA measurement is the basis for the certified SRM® 1963 particle size. Supplementary measurements, which did not provide complete uncertainty analyses were performed by Wyatt Technology[10] using field flow separation in combination with multi-angle laser-light scattering (WT-FFS),[27] and by Park Scientific[10] using atomic force microscopy on a monolayer of spheres in a hexagonally close packed array (PS-AFM). Included in Fig. 2 are dashed lines showing the combined range determined by the weighted mean and expanded uncertainties of the five measurements which stated their measurement uncertainties. All of the measurements are in excellent agreement with one another.

The largest uncertainty at this time arises from the reproducibility of the measurement. In the future, steps will be taken to reduce the contributions from contaminant particles and residual surface roughness, which are believed to be preventing us from having a lower uncertainty in this value. The presence of a low fraction of doublet particles, whose scattering is strongly dependent upon orientation, may also be contributing to the lack of reproducibility. By improving the cleanliness of the deposition area, by using higher quality silicon wafers, by reducing the deposition density, and by increasing the number of sampled spots on the wafer, we expect to be able to substantially reduce these sources of uncertainty.

The Type B uncertainties in our measurement are dominated by three sources: the optical properties of the silicon substrate, the properties of the substrate coating, and the shape of the particle. Improved information about the properties of the substrate and oxide and the particle shape are needed in order to make a significant reduction in the uncertainty obtained by a light scattering measurement.

The uncertainty claimed by The Scatter Works[10] is substantially lower than that determined for our measurements.[5] Part of this difference can be attributed to the improved conditions under which their measurements were performed. Their depositions were performed on higher quality wafers entirely in clean-room conditions, and their reproducibility therefore substantially better than that we obtained. However, their uncertainty is still less than the 1.0 nm that we would obtain if we were to remove all of our Type A uncertainties. The three largest Type B uncertainties identified in our study were not considered by The Scatter Works.[10] We therefore believe that our uncertainty analysis provides a more complete assessment of the uncertainties of the measurement.

The measurement performed by The Scatter Works[10] has one potential drawback: their measurement is only performed at two scattering angles for a fixed incident angle. They determine the particle size from the ratio of the two measured signals. While their results appear to be very good, the lack of a substantial number of degrees of freedom in the measurement can make their method susceptible to errors if other unexpected sources of scatter exist in the measurement.

The measurement geometry used by The Scatter Works[10] was optimized to yield the lowest combined uncertainty. The geometry used for our scattering measurement was not optimized to yield the lowest combined uncertainty. Since the scattering by small dielectric particles is dominated by interference between scattering of the particle and its image in the substrate, the scattering function is most strongly determined by the distance of the center of the particle from the surface. Two of the four largest uncertainties, the film properties and the particle shape, determine this effective distance, and the another, the optical properties of the substrate, further determine the strength of the image reflection.

Therefore, it is expected that changes in the scattering geometry are not likely to yield significantly improved diameter uncertainties.

6. SUMMARY

A light scattering measurement was performed from polystyrene latex spheres deposited onto silicon wafers. The results were fit to the Bobbert-Vlieger theory for light scattering from such spheres, and an analysis of the uncertainties arising from the measurement performed. The measured diameter of 99.7 nm ± 1.7 nm is in excellent agreement with other measurements. Improvements in the sample preparation are expected to reduce the primary uncertainty, which results from the variation between measurements. Ultimately, however, improvements in the uncertainty require improvements in the knowledge of the thin film optical properties, the optical properties of the substrate, and deformation of the spheres on the surface.

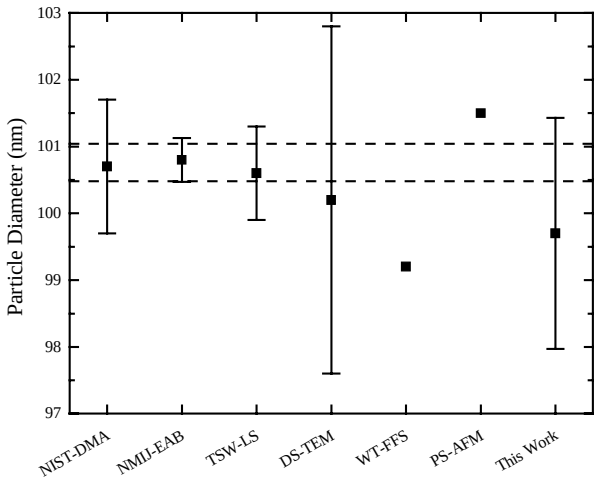

Figure 2. Summary of several measurements of the diameter of SRM® 1963. The dashed lines indicate the range resulting from a weighted average of the measurements. All of the uncertainties shown represent expanded (k=2) uncertainties.

REFERENCES AND NOTES

1. J. C. Stover, *Optical Scattering: Measurement and Analysis*, (SPIE Optical Engineering Press, Bellingham, WA, 1995).
2. B. W. Scheer, "Development of a physical haze and microroughness standard," in *Flatness, Roughness, and Discrete Defect Characterization for Computer Disks, Wafers, and Flat Panel Displays,* J. C. Stover, Ed., Proc. SPIE, **2862**, 78-95 (1996).
3. J. C. Stover and C. A. Scheer, "Accurate sizing of deposited PSL spheres from light scatter measurements," in *Optical Metrology Roadmap for the Semiconductor, Optical, and Data Storage Industries II,* A. Duparré and B. Singh, Eds., Proc. SPIE, **4449**, 147-150 (2001).
4. J. C. Stover, V. Ivakhnenko, and Y. A. Eremin, "The use of light scatter signals to identify particle material," in *Optical Metrology Roadmap for the Semiconductor, Optical, and Data Storage Industries II,* B. Singh and A. Duparré, Eds., Proc. SPIE, **4449**, 131-139 (2001).
5. Sankaran, Vijay and Stover, John C., "Advanced Particle Sizing Technique for Development of High-Accuracy Scanner Calibration Standards," Technology Transfer #99083800B-TR, (Sematech, Austin, TX, 1999).
6. P. A. Bobbert and J. Vlieger, "Light scattering by a sphere on a substrate," Physica **137A,** 209-242 (1986).
7. Y. A. Eremin, J. C. Stover, and N. V. Orlov, "Modeling scatter from silicon wafer features based on discrete sources method," Opt. Eng. **38,** 1296-1304 (1999).
8. T. Wriedt and A. Doicu, "Light scattering from a particle on or near a surface," Opt. Commun. **152,** 376-384 (1998).

9. G. W. Mulholland, N. P. Bryner, and C. Croarkin, "Measurement of the 100 nm NIST SRM 1963 by differential mobility analysis," Aerosol Sci. and Technol. **31,** 39-55 (1999).
10. Certain commercial equipment, instruments, or materials are identified in this paper in order to specify the experimental procedure adequately. Such identification is not intended to imply recommendation or endorsement by the National Institute of Standards and Technology, nor is it intended to imply that the materials or equipment identified are necessarily the best available for the purpose.
11. J. H. Kim, S. H. Ehrman, G. W. Mulholland, and T. A. Germer, "Polarized light scattering from metallic particles on silicon wafers," in *Optical Metrology Roadmap for the Semiconductor, Optical, and Data Storage Industries*, A. Duparré and B. Singh, Eds., Proc. SPIE, **4449**, 281-290 (2001).
12. J. H. Kim, S. H. Ehrman, G. W. Mulholland, and T. A. Germer, "Polarized light scattering by dielectric and metallic spheres on silicon wafers," Appl. Opt., submitted for publication (2002).
13. T. A. Germer, *SCATMECH: Polarized Light Scattering C++ Class Library* (available at http://physics.nist.gov/scatmech, 2000).
14. A. Doicu, Yu. Eremin, and T. Wriedt, "Non-axisymmetric models for light scattering from a particle on or near a plane surface," Opt. Commun. **182,** 281-288 (2000).
15. T. A. Germer and C. C. Asmail, "Goniometric optical scatter instrument for out-of-plane ellipsometry measurements," Rev. Sci. Instr. **70,** 3688-3695 (1999).
16. C. Asmail, J. Hsia, A. Parr, and J. Hoeft, "Rayleigh scattering limits for low-level bidirectional reflectance distribution function measurements," Appl. Opt. **33,** 6084-6091 (1994).
17. W. H. Press, S. A. Teukolsky, W. T. Vetterling, and B. P. Flannery, *Numerical Recipes in C: The Art of Scientific Computing*, 2nd ed. (Cambridge University, 1992).
18. B. N. Taylor and C. E. Kuyatt, "Guidelines for Evaluating and Expressing the Uncertainty of NIST Measurement Results," NIST Technical Note 1297, (NIST, Gaithersburg, 1994).
19. P. R. Bevington and D. K. Robinson, *Data Reduction and Error Analysis for the Physical Sciences*, 2nd ed. (McGraw-Hill, New York, 1992), pp. 58-60
20. E. Marx and G. W. Mulholland, "Size and refractive index determination of single polystyrene spheres," J. Res. Natl. Bur. Stand. **88,** 321-338 (1983).
21. C. M. Herzinger, B. Johs, W. A. McGahan, J. A. Woollam, and W. Paulson, "Ellipsometric determination of optical constants for silicon and thermally grown silicon dioxide via a multi-sample, multi-wavelength, multi-angle investigation," J. Appl. Phys. **83,** 3323-3336 (1998).
22. E. D. Palik, *Handbook of Optical Constants of Solids*, (Academic, San Diego, 1985).
23. T. A. Germer, "Light scattering by slightly non-spherical particles on surfaces," Opt. Lett. **27**, 1159-1161 (2002).
24. K. L. Johnson, K. Kendall, and A. D. Roberts, "Surface energy and the contact of elastic solids," Proc. R. Soc. Lond. A **324,** 301-313 (1971).
25. R. Schmehl, B. M. Nebeker, and E. D. Hirleman, "Discrete-dipole approximation for scattering by features on surfaces by means of a two-dimensional fast Fourier transform technique," J. Opt. Soc. Am. A **14,** 3026-3036 (1997).
26. K. Ehara, K. Takahata, and M. Koike, "Absolute size measurement of monodisperse particles using the electro-gravitational aerosol balance," in *20th Annual American Association of Aerosol Research Conference*, 261 (2001).
27. H. Thielking, D. Roessner, and W.-M. Kulicke, "On-line coupling of flow field-flow fractionation and multiangle laser light scattering for the characterization of polystyrene particles," Anal. Chem. **67,** 3229-3233 (1995).